Survivability Analysis of Satellite-Based Networks Under Solar Storm Hazards

Xin Guo[1], and Lisheng Ma[2]
[1]School of Systems Information Science, Future University Hakodate, 116-2
Kamedanakano-cho, Hakodate, Hokkaido, 041-8655, Japan
[2]School of Computer and Information Engineering, Chuzhou University, Chuzhou, Anhui, 239000, China

Satellite-based networks are envisioned to enable high-speed, low-latency global connectivity. However, solar storm hazards, characterized by high-energy particles, pose significant risks to satellite nodes and communication links, potentially causing network failures. Survivability assessment is crucial for evaluating the impact of such disasters on network performance and designing mitigation strategies. This study focuses on the survivability assessment of satellite networks under solar storm conditions. Specifically, we analyze the effects of solar storms on satellite networks and develop a failure model based on a regional disaster framework to quantify the probabilities of node and link capacity. Building on this model, we propose an algorithm to evaluate network survivability, encompassing metrics such as satellite survival probability, network link capacity, and routing capacity under varying solar storm intensities. The experimental results demonstrate the network's survivability under solar storm disasters of different intensities, providing a basis for developing protection strategies.

***Index Terms*—Solar storm disaster, satellite networks, survivability assessment, region failure model.**

I. Introduction

SATELLITE networks, particularly Low Earth Orbit (LEO) satellite constellations, are pivotal in enabling high-speed, low-latency global connectivity. These networks typically consist of numerous satellites operating in coordinated orbits, interconnected via inter-satellite links, and communicating with ground stations and user terminals. This architecture supports applications such as global Internet coverage, real-time data transmission, and edge computing. However, these networks are vulnerable to natural hazards, such as solar storms, which pose significant threats to their operation[1]. Solar storms, characterized by high-energy particles and electromagnetic disturbances, can damage satellite nodes and disrupt communication links, leading to potential network outages or failures[2]. Therefore, understanding the basic structure and functioning of satellite networks, as well as their survivability under such adverse conditions, is essential for ensuring reliability and designing effective protection strategies[3], [4].

Existing research has addressed several aspects of solar storm observation and prediction[5], fault modeling for satellite networks[3], and general network survivability assessment. However, challenges remain in accurately modeling the regional impacts of solar storms and translating failure probabilities into actionable network performance metrics. Additionally, there is limited research on survivability assessment tailored to satellite networks under solar storm hazards.

In this study, we aim to bridge these gaps by proposing a comprehensive survivability assessment framework for satellite networks under solar storms. Specifically, we develop a failure model based on a regional disaster framework, calculate node and link failure probabilities, and evaluate network performance through metrics such as survival probability, connectivity, routing robustness, and throughput. The experimental results reveal key patterns of network performance degradation under varying solar storm intensities, providing valuable insights for designing mitigation strategies.

The rest of this paper is organized as follows: Section II reviews related work, including solar storm observation and prediction, satellite network fault modeling, and survivability assessment methods. Section III presents our fault model for assessing node and link failure probabilities. Section IV introduces the survivability assessment algorithm and its key components. Section V discusses experimental results and insights derived from the analysis. Finally, Section VI concludes the paper and outlines future directions for this research.

II. Related Work

A. The Vulnerability of Satellite Networks Under Extreme Events

Satellite network vulnerability refers to the susceptibility of satellite systems to failures caused by various factors, including system faults, human-induced attacks, and natural disasters [6]. System faults, such as hardware degradation or software errors, often result in partial or complete service disruptions [7], [8]. Human-induced threats, such as cyber attacks or physical tampering, aim to compromise the network's confidentiality, integrity, or availability [9]. Meanwhile, natural disasters, including solar storms, meteor showers, and extreme weather conditions, exacerbate the vulnerability by introducing stochastic and often unpredictable risks.

The metrics used to measure vulnerability include connectivity loss [10], communication delay [7], and system robustness under stress conditions. Understanding these vulnerabilities is critical for designing resilient satellite networks that maintain functionality even in adverse environments [11].

Research on satellite network reliability focuses on fault-tolerant designs, redundancy mechanisms, and self-healing

Manuscript received December 18, 2024; revised January 20, 2025. Corresponding author: Guo Xin (email: guoxin167@126.com).

capabilities. These studies aim to ensure uninterrupted services despite internal failures [7], [8], [11]. Studies explore the impact of cyber and physical attacks on satellite networks, including jamming, spoofing, and denial-of-service (DoS) attacks. Techniques like secure routing protocols and encryption algorithms have been proposed to mitigate these threats [9], [12]. Natural disasters, especially space weather events like solar storms, pose unique challenges. Recent work has investigated the effects of solar particle radiation and geomagnetic disturbances on satellite hardware and inter-satellite links, emphasizing the need for real-time monitoring and adaptive control strategies.

B. Solar Storms and Their Impact on the Space Environment

Solar storms encompass a variety of solar activities that release massive amounts of energy into space. The primary types include Coronal Mass Ejections (CMEs), Solar Energetic Particle (SEP) Events and Solar Flares. Solar storms are classified according to their intensity and their impact on the Earth's geomagnetic environment, including A, B, C, M, and X (solar flares)[1], [13], [2].

Energetic particles from SEPs can penetrate satellite shielding, causing Single Event Upsets (SEUs) and Total Ionizing Dose (TID). SEUs bit flips in memory and processing units. TID accumulated radiation damage over time, degrading satellite electronics [14], [15]. Increased solar activity heats the Earth's upper atmosphere, causing it to expand. This leads to heightened drag on LEO satellites, accelerating orbital decay and requiring more frequent station-keeping maneuvers [16]. Geomagnetic storms caused by CMEs or solar flares can induce errors in satellite navigation systems (e.g., GPS signal degradation) and communication blackouts due to ionospheric disturbances [17], [18].

Solar storm monitoring relies on advanced space-based instruments. SOHO (Solar and Heliospheric Observatory) monitors the Sun's atmosphere and captures CME dynamics [19]. ACE (Advanced Composition Explorer) measures solar wind particles and magnetic fields near earth [20]. Prediction models like the NELIL (Near-Earth Location-Intensity-Lifetime) model use inputs such as initial solar wind speed, density, and magnetic field strength to estimate solar wind propagation and predict storm impacts. These models provide essential warnings to satellite operators and infrastructure managers [5].

C. Vulnerability Assessment Models and Methods

Failure modeling in satellite networks often employs node failure [3], [4], link failure [21], regional failure [22], [23], [24], and cascading failure models [25] to represent different scenarios.

Node failure models [3], [4] are applicable to scenarios where individual satellite failures occur due to hardware malfunctions, software bugs, or limited energy resources. Such models are frequently used to analyze satellite constellations' survivability under isolated failures.

Link failure models [21] focus on disruptions in inter-satellite or satellite-to-ground communication links caused by antenna misalignment, atmospheric interference, or hardware damage. These models are useful for evaluating routing protocols and communication reliability.

Regional failure models [22], [23], [24] are designed for large-scale scenarios, such as natural disasters (e.g., hurricanes or geomagnetic storms), affecting multiple satellites or ground nodes within a geographic area.

Cascading failure models [25] are critical for assessing failure propagation in highly interconnected networks, such as densely packed satellite constellations or multi-layer networks. They help identify weak points in the network topology that may amplify small failures into widespread disruptions.

By aligning each model with specific failure scenarios, researchers can select appropriate methods based on the system's design and expected challenges.

Simulation-based techniques utilize tools like NS3, OPNET, or MATLAB/Simulink to model satellite networks and simulate the impacts of failures such as those caused by solar storms. These methods excel in providing detailed insights into network performance under specific failure conditions and allow for visualizing network changes dynamically. However, they come with high computational costs and limited scalability, especially for large-scale networks. Simulation approaches are best suited for testing new protocols or resilience strategies in specific scenarios.

Analytical methods use mathematical and probabilistic models to assess satellite network survivability and robustness. These models are computationally efficient and suitable for large networks, making them ideal for high-level vulnerability assessments or design feasibility studies. However, they often simplify network behaviors and may not effectively capture dynamic phenomena like cascading failures. Analytical approaches are most effective during the early design stages or for generalized studies.

Empirical studies analyze historical data from past satellite failures or solar storm events. They offer high realism and practical insights, serving as benchmarks for simulations or validations for analytical models. Nevertheless, they are limited by the availability and relevance of data and lack predictive capabilities for novel failure scenarios. Empirical approaches are commonly employed for retrospective analysis and model calibration.

Each method has distinct strengths and weaknesses. Simulation-Based approaches provide detailed and dynamic results but require significant computational resources. Analytical models offer scalability and efficiency, though they lack the detailed realism of simulations. Empirical studies are grounded in real-world data but are constrained by dataset availability and historical scope.

Simulation-Based methods use these for scenario-specific testing of protocols or strategies. Analytical models apply them for large-scale, high-level evaluations during network design. Empirical studies leverage these for validating models and deriving insights from historical events.

Compared to simulation-based methods, our approach is more scalable and suitable for large networks. Compared to analytical methods, it offers greater detail and dynamic adaptability. However, unlike empirical studies, it lacks grounding in historical data, which could enhance its realism.

III. System Model

A. Network Model

Consider a three-layer heterogeneous satellite network as shown in Fig. 1, which consists of N_L LEO satellites, N_M MEO satellites, N_G GEO satellites and N_{GS} ground stations . Satellites in the same layer are connected by same-layer inter-satellite links (SL-ISLs), while satellites and ground stations in different layers are connected by cross-layer links (CLLs). All links in the network are bidirectional. Satellites and ground stations are abstracted as nodes and links between satellites and satellite-to-ground as edges. The network can be modeled by a multi-layer graph as $G = (V, E)$, where

$V = \{V_L, V_M, V_G, V_{GS}\}$ is the set of all nodes.

$E = \{e(u, v)|, u \neq v\}$ is the set of all edges. $e(u, v) = 1$ represents that there exists a link between u and v, while $e(u, v) = 0$ represents that there is no link between u and v.

The average number of connections for same-layer and cross-layer links is given by: $N^L_{SL-ISL} = 4, N^M_{SL-ISL} = 2$, and $N^G_{SL-ISL} = 4$ represent the number of same-layer connections of LEO, MEO, and GEO, respectively. $N^{L,M}_{CLL} = 2, N^{M,G}_{CLL} = 2$, and $N^{GS,L}_{CLL} = 4$ represent the number of cross-layer connections of LEO-to-MEO, MEO-to-GEO, and LEO satellite to GS, respectively.

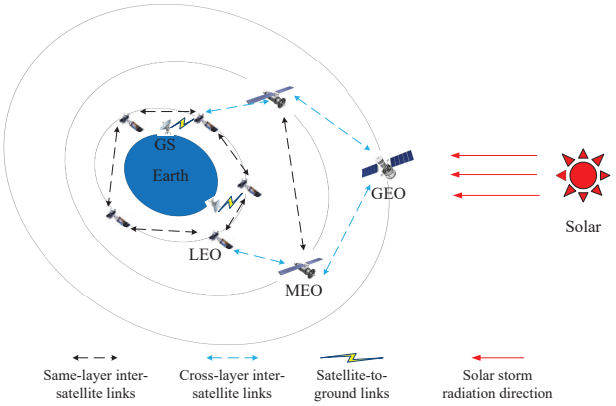

Fig. 1. Multi-layer satellite networks.

In the related literature, only some satellite nodes maintain cross-layer links. The setting of this paper is similar [26]. As mentioned above, the satellite network is a multi-layer network composed of two aspects, the first of which is the node type and the second is time. Since MEO and LEO satellites move around the earth periodically, the edges in the satellite network will change over time. Assume that there are N_T topologies during time T, and the time duration of the t-th topology is T_t, where the constraint $\sum_{t=1}^{N_T} T_t = T$ is naturally satisfied. Then the edges in the satellite network are redefined as 1

$$E = \{e(u, v, t)|, u \neq v, t \in [1, N_T]\}. \quad (1)$$

B. Regional failure model under solar storm

By constructing a solar storm regional failure model, we evaluate the occurrence probability and impact of faults in a specific region. As shown in Fig. 2, the solar storm disaster model based on solar storm divides the disaster into multiple concentric classes with the sun as the disaster center. Different concentric classes represent different distances, and when determining the fault probability in different regions, we obtain the Probability Region Failure (PRF) of nodes and links.

The PRF is defined by a continuous spherical shell, with radius r_i and i. The i-th layer of the spherical shell is associated with a failure probability p_i, which decreases monotonically as the radius of the shell increases. For example, $p_i \geq p_(i+1), (1 \leq i \leq m-1)$. Here, the domain is restricted to a spherical region of radius r_3, beyond which the failure probability is considered to be zero.

The regional failure probability p_i is related to the solar storm intensity D (unit: W/m^2). The solar storm speed s, particle density n, and magnetic field strength B at any position in space are calculated based on the solar storm intensity.

The initial solar storm speed $s_0(km/s)$, particle density

TABLE I
List of Symbols

Symbol	Description
N_L	Number of LEO satellites
N_M	Number of MEO satellites
N_G	Number of GEO satellites
N_{GS}	Number of ground stations
N_{SL-ISL}	Average number of same-layer links
N^L_{SL-ISL}	Number of links for LEO satellites
N^M_{SL-ISL}	Number of links for MEO satellites
N^G_{SL-ISL}	Number of links for GEO satellites
N_{CLL}	Average number of cross-layer links
$N^{L,M}_{CLL}$	Number of cross-layer links between LEO and MEO satellites
$N^{M,G}_{CLL}$	Number of cross-layer links between MEO and GEO satellites
$N^{GS,L}_{CLL}$	Number of cross-layer links between ground stations and LEO satellites
T	Total time period
T_t	Time duration of the t-th topology
N_T	Number of topologies during time T
r	Distance from the sun (AU)
r_i	Radius of the i-th spherical shell
p_i	Failure probability of the i-th spherical shell
s_r	Solar storm speed at distance r
n_r	Particle density at distance r
B_r	Magnetic field strength at distance r
s_0	Initial solar storm speed
n_0	Initial particle density
B_0	Initial magnetic field strength
m_p	Proton mass (1.67×10^{-27} kg)
μ_0	Vacuum permeability ($4\pi \times 10^{-7}$ H/m)
D^r_X	Solar storm intensity in region r
α, β, γ	Empirical parameters for failure probability
P^r_X	Failure probability at distance r under solar storm intensity X

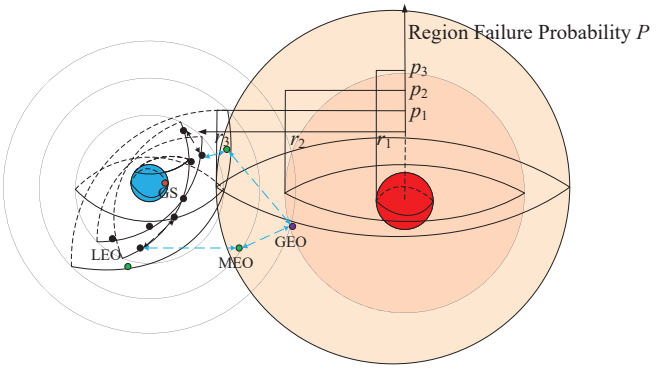

Fig. 2. Regional failure model under solar storm, m=3.

$n_0(particles/cm^3)$, and magnetic field strength $B_0(nT)$ can be obtained based on the solar storm intensity. Here is how to calculate the solar storm speed, particle density, and magnetic field strength at any location. The speed s_r of the solar storm is obtained by 2, where r_0 is initial propagation distance (usually set to 0.1AU), k is deceleration factor (empirical value is 20 km/s/AU). Arrival time t_a at any location can be calculate as 3. The formulas for calculating particle density n_r and magnetic field strength B_r are shown in 4 and 5.

$$s_r = s_0 - k \cdot (r - r_0). \tag{2}$$

$$t_a = \frac{1}{k} \ln \frac{s_0}{s_r} + \frac{r - r_0}{s_r}. \tag{3}$$

$$n_r = n_0 (\frac{r - r_0}{r})^2. \tag{4}$$

$$B_r = B_0 (\frac{r - r_0}{r})^2. \tag{5}$$

D_X^r is the sum of the kinetic energy flow and magnetic field energy carried by region r when the solar storm intensity is level X, and is mainly composed of the following two parts as 6 kinetic energy density $\frac{1}{2} n m_p v_r^3$ and magnetic field energy density $\frac{B_r^2}{2\mu_0}$, where proton mass $m_p = 1.67 \times 10^{-27} kg$ and vacuum permeability $\mu_0 = 4\pi \times 10^{-7} H/m$.

$$D_X^r = \frac{1}{2} n m_p v_r^3 + \frac{B_r^2}{2\mu_0}. \tag{6}$$

Assuming that the particle kinetic energy dominates the power density, that is, ignoring the magnetic field energy term (this assumption is applicable to most solar wind calculations), the initial solar velocity can be calculated as shown in the formula $s_0 = (\frac{2D_X^r}{n_0 m_p})^{\frac{1}{3}}$. Typical particle density $n_0 = 5 \times 10^{12} particles/m^3$ (Common values for low earth orbit). Calculate the magnetic field strength $B_0 = (0.2\mu_0 D_X^r)^{\frac{1}{2}}$, for example, the magnetic field energy usually accounts for about 10% of the total power.

The failure probability at any position r is related to the solar wind speed, magnetic field strength, and particle density, and the calculation formula is as follows 7. α, β, γ empirical parameters used to measure the impact of velocity, particle density and magnetic field on failure probability.

$$P_X^r = 1 - exp(-\alpha v_r - \beta n_r - \gamma B_r^2). \tag{7}$$

The algorithm 1 computes the failure probability $P_{D_i}^r$ in various regions under different intensities of solar storms ($\{D_A, D_B, D_C, D_M, D_X\}$). By iterating over solar storm intensity classes and spatial regions, it calculates the plasma properties (s_r, n_r, B_r) and derives the probability of satellite failures using a mathematical model.

Algorithm 1 Calculation of PRF under different solar storm intensities

Input: The intensity of solar storms D_A, D_B, D_C, D_M, D_X.
Output: Failure probability at different strengths and in different regions $P_{D_i}^r$.
for each class $D_i \in \{D_A, D_B, D_C, D_M, D_X\}$ **do**
  $s_0 = (\frac{2D_i}{n_0 m_p})^{\frac{1}{3}}$
  $B_0 = (0.2\mu_0 D_i)^{\frac{1}{2}}$
  for each r **do**
    $s_r = s_0 - k \cdot (r - r_0)$
    $n_r = n_0 (\frac{r - r_0}{r})^2$
    $B_r = B_0 (\frac{r - r_0}{r})^2$
    $P_{D_i}^r = 1 - exp(-\alpha v_r - \beta n_r - \gamma B_r^2)$
  end for
end for

IV. Survivability Assessment Algorithm

A. Calculation of node or link failure probability

Algorithm 2 Calculate the failure probability of satellite nodes

Input: Failure probability at different strengths and in different regions $P_{D_i}^r$ and satellite node location information V_t at t-th topology.
Output: Failure probability of each satellite node P_t^v in different topologies.
for each topology node set V_t **do**
  for each node v **do**
    Calculate the distance d between the satellite v and the failure center r_0.
    Determine the failure area v_r where the node v is located based on the distance d.
    $p_v = P_{D_i}^{v_r}$
  end for
end for

Node failure is expressed as the failure probability P_v of node v in the i-th sphere as follows:

$$P_v = p_i. \tag{8}$$

This algorithm 2 determines the failure probability p_v for each satellite node in different network topologies. Based on satellite positions and the failure center r_0, it calculates the distance, identifies the failure region, and assigns the corresponding failure probability from $P_{D_i}^r$.

Since satellite links are wireless communication links, we use degradation in wireless communication link capacity to assess the impact of disasters on the links. The initial capacity of the link e is C_e. Then the proportion of the degradation capacity of link e, P_{f_e}, can be expressed as:

$$P_{f_e} = \sum_{j=1}^{K} \frac{d_j}{D} p_{e_j}. \tag{9}$$

K represents the number of link divisions, D is the total length of the link, d_j represents the length of the j-th segment, and p_{e_j} is the failure probability of the j-th segment on link e.

The algorithm 3 evaluates the degradation rate p_e of satellite link capacity in various topologies. By segmenting each link and calculating its proximity to the failure center r_0, it identifies the relevant failure region and aggregates the degradation rate for all link segments to estimate the overall link degradation rate.

Algorithm 3 Calculate the degradation rate of satellite link capacity

1: **Input:** Failure probability at different strengths and in different regions $P^r_{D_i}$ and satellite link location information E_t at t-th topology.
2: **Output:** The degradation rate of each satellite links P^e_t in different topologies.
3: **for** each topology link set E_t **do**
4: **for** each link e **do**
5: Segment the link e.
6: Calculate the distance d between the link e_i and the failure center r_0.
7: Determine the failure area e^r_i where the link e_i is located based on the distance d.
8: $p_e = \sum_{j=1}^{K} \frac{d_j}{D} p_{e_j}$.
9: **end for**
10: **end for**

B. Algorithms for evaluating network survivability

The algorithm 4 calculates the bandwidth degradation ratio P^r_t of routing paths in a given topology. By considering the bandwidth degradation of links in each path, a probabilistic model is used to estimate the overall path reliability.

Algorithm 4 Calculate the degradation rate of of path capacity

1: **Input:** Failure probability of each satellite node P^v_t and failure probability of each satellite links P^e_t in the topology t. The set of routing path R_t.
2: **Output:** The degradation rate of each path P^r_t in topology t.
3: **for** each path $pr \in P^r_t$ **do**
4: The set of nodes V_{pr} and links E_{pr} that the path passes through.
5: $p_{pr} = \min_{e \in E_{pr}} (p_e = \sum_{j=1}^{K} \frac{d_j}{D} p_{e_j})$.
6: **end for**

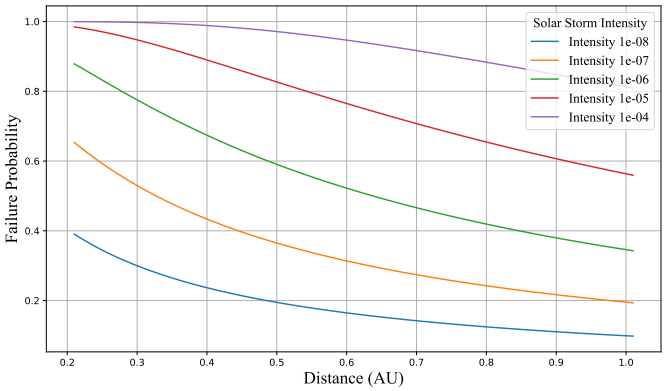

Fig. 3. Failure Probability vs Distance for Different Solar Storm Intensities.

V. Numerical Simulation Results

A. Experimental setup

The satellite network was created based on the NeLS [27] constellation and the simulation environment was created using SGP4 and GMAT. As shown in Table II, the intensity classification of solar storms and the value range of each category are given [2].

TABLE II
Solar Storm Intensity Classification

Category	Intensity (W/m^2)
A	$10^{-8} \sim 10^{-7}$
B	$10^{-7} \sim 10^{-6}$
C	$10^{-6} \sim 10^{-5}$
M	$10^{-5} \sim 10^{-4}$
X	$10^{-4} <$

In this study, all satellite nodes and links are assumed to have the same level of disaster resistance. In this study, our path evaluation prioritizes the shortest path, and randomly selects 6 shortest paths for evaluation.

As shown in the Fig. 3, the impact of solar storms of different intensities on the failure probability of varying distances from the sun is studied. By constructing a failure model and combining the attenuation rules of solar storm parameters (wind speed, particle density, magnetic field strength) with distance r, the failure probability at different distances is calculated. The experiment examined five scenarios of different solar storm intensities.

The experimental results show the failure probability as a function of solar distance (AU). For higher-intensity solar storms, the failure probability increases rapidly at shorter distances and tends to saturation, while for lower-intensity solar storms, the failure probability increases more slowly and is generally lower. The curve reveals that the higher the intensity of the storm, the more significant the impact will be on areas closer to the sun. The intensity of solar storms is a key factor in determining the reliability of communications equipment or satellite networks, especially at shorter distances. More efficient shielding or failure recovery mechanisms need to be designed for high intensity storms.

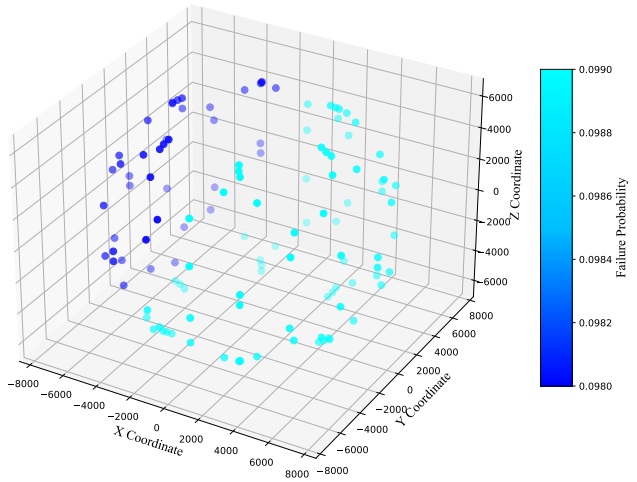

Fig. 4. Failure probability of satellite nodes under Class A solar storm.

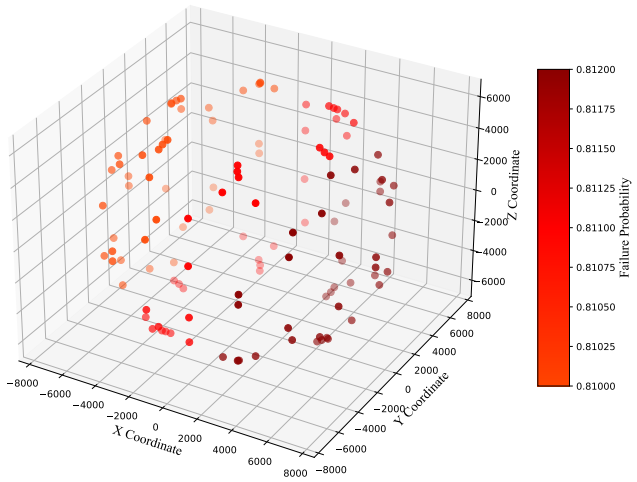

Fig. 5. Failure probability of satellite nodes under Class X solar storm.

B. Node failure probability analysis

As shown in Fig. 4 and Fig. 5, the failure probability distribution of satellite nodes under solar storm intensities A and X is visualized. By inputting the spatial position of the satellite and the corresponding failure probability data, a three-dimensional scatter plot is used to show the difference in node distribution and its failure probability.

The position distribution and failure probability of each satellite node can be observed through the scatter plot. The difference in satellite failure probability is reflected by the color gradient, and the darker the color, the higher the failure probability. The failure probability of A-level solar storms is generally low, concentrated between 0.098 and 0.099. The failure probability of X-level solar storms is generally high, concentrated between 0.810 and 0.812.

Solar storms with lower intensity pose limited threats to satellite nodes, while high-intensity solar storms have a serious impact on satellite nodes. In addition, the location of satellite nodes will also affect the failure probability of nodes. It emphasizes the importance of enhancing the anti-interference capability of satellite systems under extreme space weather conditions.

C. Link capacity degradation rate analysis

As shown in Fig. 6 and Fig. 7, the degradation rate distribution of satellite links capacity under solar storm intensities A and X is visualized. By inputting the location of the satellite link and the corresponding failure probability data, a three-dimensional scatter plot is used to show the difference in link distribution and its degradation rate.

The difference in satellite link capacity degradation rate is reflected by the color gradient, and the darker the color, the higher the capacity degradation rate. The capacity degradation rate of A-level solar storms is generally low, concentrated between 0.188 and 0.187. The capacity degradation rate of X-level solar storms is generally high, concentrated between 0.963 and 0.965.

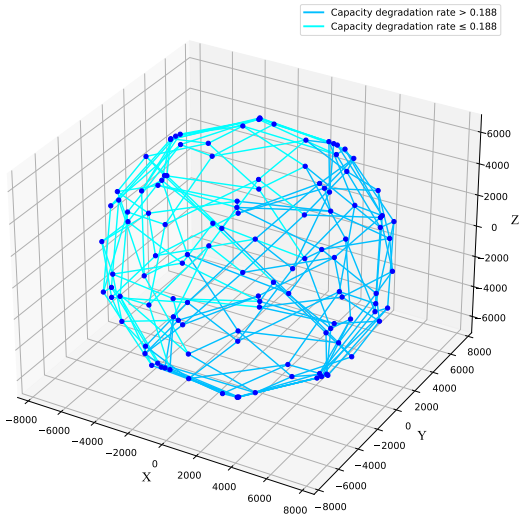

Fig. 6. Capacity degradation rate of satellite links under Class A solar storm.

The experimental results show that under the same intensity, the capacity degradation rate of the link is higher than the failure probability of the node. Solar storms with lower intensity have limited threats to satellite links, while high-intensity solar storms have serious effects on satellite links. In addition, the location of the satellite link will also affect the capacity degradation rate of the link. It emphasizes the importance of enhancing the anti-interference capability of satellite links under extreme space weather conditions.

D. Path capacity degradation rate analysis

As shown in Fig. 8 and Fig. 9, the capacity degradation rate distribution of satellite routing paths under solar storm intensities A and X is visualized. By inputting the location of the satellite path and the corresponding data, a three-dimensional scatter plot is used to show the difference in path distribution and its capacity degradation rate.

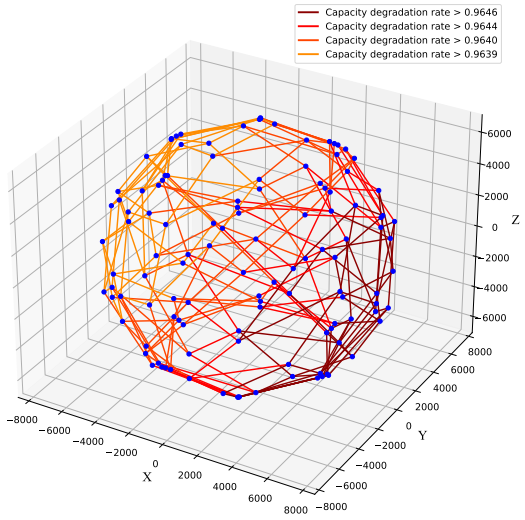

Fig. 7. Capacity degradation rate of satellite links under Class X solar storm.

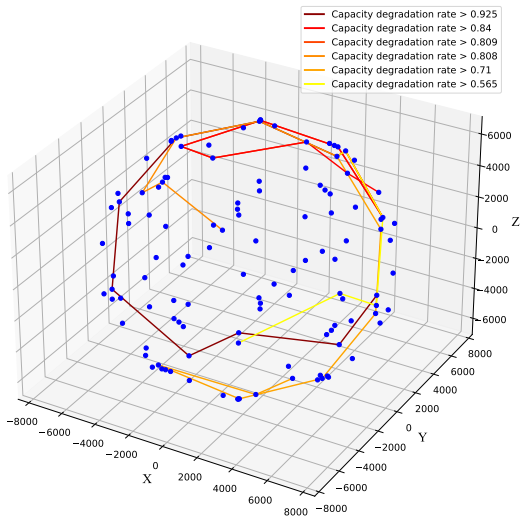

Fig. 8. Capacity degradation rate of satellite paths under Class A solar storm.

The difference in satellite path capacity degradation rate is reflected by the color gradient, and the darker the color, the higher the capacity degradation rate. The capacity degradation rate of A-level and X-level solar storms is generally high, concentrated between 0.565 and 0.925, or bigger than 0.99.

The experimental results show that under the same intensity, the capacity degradation rate of the path is higher than the failure probability of the node and the capacity degradation rate of link. Solar storms with lower intensity or high intensity solar storms have serious effects on satellite paths. In addition, the number of the satellite path's nodes and links will also affect the capacity degradation rate of the path. It emphasizes the importance of enhancing the anti-interference capability of satellite routing paths under extreme space weather conditions.

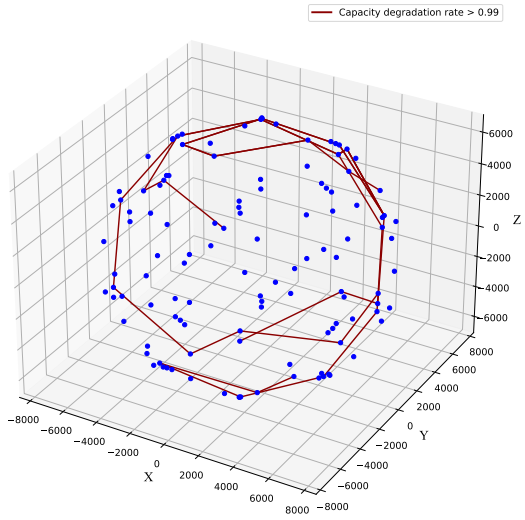

Fig. 9. Capacity degradation rate of satellite paths under Class X solar storm.

VI. Conclusion

This paper preliminarily discusses the survivability of satellite networks under solar storm disasters. A regional failure model based on the intensity of solar storms is established, and the failure probability of satellite nodes, links and paths capacity degradation rate in the satellite network is evaluated. The experimental results show the vulnerability of satellite networks under solar storm disaster scenarios, providing a basis for subsequent research on protection strategies.

References

[1] A. K. Singh, A. Bhargawa, D. Siingh, and R. P. Singh, "Physics of space weather phenomena: a review," *Geosciences*, vol. 11, no. 7, p. 286, 2021.

[2] K. Omatola and I. Okeme, "Impacts of solar storms on energy and communications technologies," *Archives of Applied Science Research*, vol. 4, no. 4, pp. 1825–1832, 2012.

[3] X. Xu, Z. Gao, and A. Liu, "Robustness of satellite constellation networks," *Computer Communications*, vol. 210, pp. 130–137, 2023.

[4] S. Li, C. Zhang, C. Zhao, and C. Xia, "Analyzing the robustness of leo satellite networks based on two different attacks and load distribution methods," *Chaos: An Interdisciplinary Journal of Nonlinear Science*, vol. 34, no. 3, 2024.

[5] Space Weather Prediction Center (SWPC), "Wsa-enlil solar wind prediction," 2016. [Online]. Available: https://www.swpc.noaa.gov/products/wsa-enlil-solar-wind-prediction

[6] M. S. Hossain, S. S. Hassan, M. Atiquzzaman, and W. Ivancic, "Survivability and scalability of space networks: a survey," *Telecommunication Systems*, vol. 68, pp. 295–318, 2018.

[7] K.-C. Tsai, L. Fan, R. Lent, L.-C. Wang, and Z. Han, "Distributionally robust optimal routing for integrated satellite-terrestrial networks under uncertainty," *IEEE Transactions on Communications*, 2024.

[8] X. Fan, D. Liu, M. Qiu, Y. Li, J. Huo, H. Li, and C. Sun, "Dynamic prioritized data transmission through inter-satellite cooperation in leo constellations," *IEEE Internet of Things Journal*, 2024.

[9] A. Toubi and A. Hajami, "Vulnerability assessment and mitigation strategies for satellite communication systems under ddos attacks," in *2024 International Conference on Global Aeronautical Engineering and Satellite Technology (GAST)*. IEEE, 2024, pp. 1–8.

[10] G. Boquet, B. Martinez, F. Adelantado, J. Pages, J. A. Ruiz-de Azua, and X. Vilajosana, "Low-power satellite access time estimation for internet of things services over non-terrestrial networks," *IEEE Internet of Things Journal*, 2023.

[11] R. Wang, M. A. Kishk, and M.-S. Alouini, "Reliability analysis of multi-hop routing in multi-tier leo satellite networks," *IEEE Transactions on Wireless Communications*, 2023.
[12] R. L. Gobbi, E. Schaefer, J. Jacobs, and D. Street, "Satellite communications resilience–service restoration and retainment," in *MILCOM 2023-2023 IEEE Military Communications Conference (MILCOM)*. IEEE, 2023, pp. 371–376.
[13] R. Miteva, S. W. Samwel, and S. Tkatchova, "Space weather effects on satellites," *Astronomy*, vol. 2, no. 3, pp. 165–179, 2023.
[14] S. W. Samwel, E. A. El-Aziz, H. B. Garrett, A. A. Hady, M. Ibrahim, and M. Y. Amin, "Space radiation impact on smallsats during maximum and minimum solar activity," *Advances in Space Research*, vol. 64, no. 1, pp. 239–251, 2019.
[15] P. Hajipour, M. Danaeefar, M. Ebrahimzadeh, and S. Radiom, "Space environment and evaluation of typical high altitude satellite," *Journal of Iranian Association of Electrical and Electronics Engineers*, vol. 10, no. 2, pp. 49–56, 2013.
[16] V. Wilken, M. Kriegel, N. Jakowski, and J. Berdermann, "An ionospheric index suitable for estimating the degree of ionospheric perturbations," *Journal of Space Weather and Space Climate*, vol. 8, p. A19, 2018.
[17] J. C. Valdés Abreu, "Degradation of the global navigation satellite system positioning accuracy caused by ionospheric disturbance sources," 2023.
[18] C. López-Urias, G. E. Vazquez-Becerra, K. Nayak, and R. López-Montes, "Analysis of ionospheric disturbances during x-class solar flares (2021–2022) using gnss data and wavelet analysis," *Remote Sensing*, vol. 15, no. 18, p. 4626, 2023.
[19] W. Finsterle, J. P. Montillet, W. Schmutz, R. Šikonja, L. Kolar, and L. Treven, "The total solar irradiance during the recent solar minimum period measured by soho/virgo," *Scientific reports*, vol. 11, no. 1, p. 7835, 2021.
[20] A. Poppe, P. Szabo, E. Imata, L. Keller, and R. Christoffersen, "Solar-energetic-particle track-production rates in interplanetary dust grains at 1 au," in *55th Lunar and Planetary Science Conference (LPSC)*. Lunar and Planetary Institute, 2024.
[21] Z. Lai, H. Li, Y. Wang, Q. Wu, Y. Deng, J. Liu, Y. Li, and J. Wu, "Achieving resilient and performance-guaranteed routing in space-terrestrial integrated networks," in *IEEE Conference on Computer Communications*, 2023, pp. 1–10.
[22] X. Wang, X. Jiang, and A. Pattavina, "Assessing network vulnerability under probabilistic region failure model," in *2011 IEEE 12th International Conference on High Performance Switching and Routing*. IEEE, 2011, pp. 164–170.
[23] L. Ma, X. Jiang, B. Wu, A. Pattavina, and N. Shiratori, "Probabilistic region failure-aware data center network and content placement," *Computer Networks*, vol. 103, pp. 56–66, 2016.
[24] J. Liu, X. Jiang, H. Nishiyama, and N. Kato, "Reliability assessment for wireless mesh networks under probabilistic region failure model," *IEEE Transactions on Vehicular Technology*, vol. 60, no. 5, pp. 2253–2264, 2011.
[25] L. Zhang and Y. Du, "Cascading failure model and resilience enhancement scheme of space information networks," *Reliability Engineering & System Safety*, vol. 237, p. 109379, 2023.
[26] X. Zhu, C. Jiang, L. Kuang, M. Dong, and Z. Zhao, "Capacity analysis of multi-layer satellite networks," in *2020 International Wireless Communications and Mobile Computing (IWCMC)*. IEEE, 2020, pp. 251–256.
[27] R. Suzuki and Y. Yasuda, "Study on isl network structure in leo satellite communication systems," *Acta Astronautica*, vol. 61, no. 7-8, pp. 648–658, 2007.

Xin Guo received the B.S. and M.S. degrees from Datong University, China in 2019 and from Xidian University, China in 2023, respectively. He is currently pursuing a Ph.D. degree at the School of Systems Information Science, Future University Hakodate, Japan. His research focuses on the survivability of satellite-terrestrial networks.

Lisheng Ma received the B.S., M.S. and Ph.D. degrees from Taiyuan Normal University, China in 2004, from Southwest University, China in 2007 and from Future University Hakodate, Japan in 2017, respectively. He is currently a professor of Chuzhou University, China. His research interests include network survivability and network performance analysis.